The Astrophysical Journal Letters, 883:L6 (6pp), 2019 September 20 https://doi.org/10.3847/2041-8213/ab3f2c

Did GW170817 Harbor a Pulsar?

Enrico Ramirez-Ruiz[1,2], Jeff J. Andrews[2], and Sophie L. Schrøder[2]
[1] Department of Astronomy and Astrophysics, University of California, Santa Cruz, CA 95064, USA
[2] Niels Bohr Institute, University of Copenhagen, Blegdamsvej 17, DK-2100 Copenhagen, Denmark
Received 2019 May 22; revised 2019 August 28; accepted 2019 August 28; published 2019 September 17

Abstract

If the progenitor of GW170817 harbored a pulsar, then a Poynting flux dominated bow-shock cavity would have been expected to form around the traveling binary. The characteristic size of this evacuated region depends strongly on the spin-down evolution of the pulsar companion, which in turn depends on the merging timescale of the system. If this evacuated region is able to grow to a sufficiently large scale, then the deceleration of the jet, and thus the onset of the afterglow, would be noticeably delayed. The first detection of afterglow emission, which was uncovered 9.2 days after the γ-ray burst trigger, can thus be used to constrain the size of a preexisting pulsar-wind cavity. We use this information, together with a model of the jet to place limits on the presence of a pulsar in GW170817 and discuss the derived constraints in the context of the observed double neutron star binary population. We find that the majority of Galactic systems that are close enough to merge within a Hubble time would have carved a discernibly large pulsar-wind cavity, inconsistent with the onset timescale of the X-ray afterglow of GW170817. Conversely, the recently detected system J1913+1102, which hosts a low-luminosity pulsar, provides a congruous Milky Way analog of GW170817's progenitor model. This study highlights the potential of the proposed observational test for gaining insight into the origin of double neutron star binaries, in particular if the properties of Galactic systems are representative of the overall merging population.

Key words: binaries: close – gamma-ray burst: general – pulsars: general – stars: magnetars

1. Introduction

Since the discovery of the first double neutron star (DNS) binary by Hulse & Taylor (1975), a total of 18 additional systems have been uncovered by radio surveys (Stovall et al. 2018). Although these double neutron star binaries will not merge for tens of millions of years (Burgay et al. 2003; Kim et al. 2015), they make it clear that such mergers were an inescapable aftermath of binary stellar evolution (Tauris et al. 2017).

The potential outcomes arising from the merger of compact binaries was first discussed by Lattimer & Schramm (1976). They studied the tidal disruption of a neutron star by a black hole and, although they claimed that the occurrence rate was likely too rare for them to explain the then recently discovered γ-ray burst sources (Klebesadel et al. 1973), enough material might be ejected from these systems to be a primary channel for heavy element nucleosynthesis. In almost a literal sense, Lattimer & Schramm (1976) set the stage for interpreting the exceptional discovery of GW170817 (Abbott et al. 2017a). Through the unprecedented monitoring efforts of GW170817 by the astronomical community (Abbott et al. 2017b; Coulter et al. 2017), there is now a consensus that neutron star mergers can synthesize copious amounts of *r*-process material (Kasen et al. 2017) and trigger short γ-ray bursts (sGRBs; or at least a class of them; Abbott et al. 2017c).

Observing such systems before they merge can provide us with key information about the physics of binary stellar evolution and the types of gravitational-wave signals we might expect to uncover with current and future observatories (Kalogera et al. 2001). Progress is currently hampered by the small number of systems uncovered (Stovall et al. 2018), which represents a minuscule fraction of the total estimated population (Scholz et al. 2015). However, the future holds enormous promise for the study of neutron star binaries due to the advent of large wide-field radio surveys and the nascent field of gravitational-wave astronomy, which will allow the study of these populations in great detail. A combination of finding more systems before and after they merge has a great potential for constraining binary evolution but also uncovering fundamental physics of the merger. This motivates us to explore potential constraints on the premerger properties of the progenitor system of GW170817.

In this Letter we examine the consequences of the hypothesis that GW170817's progenitor system hosted a pulsar. In Section 2 we show that if a pulsar is present in the system, then a Poynting flux dominated cavity would have formed in its surroundings, effectively displacing the interstellar medium. After a review of the relevant observations, in Section 3 we examine the conditions required for a pulsar-wind cavity to grow to a sufficiently large size in order to prevent the deceleration of the relativistic ejecta in GW170817 and, as a result, delay the onset of the afterglow emission (Holcomb et al. 2014). We use this information, together with a model of the structure of the evacuated cavity to place stringent limits on the presence of a pulsar in GW170817. Finally, in Section 4 we discuss the derived constraints in the context of the observed binary neutron star population and determine the properties of the electromagnetic signatures expected from gravitational-wave sources harboring pulsars.

2. The Premerger Environment of GW170817

The optical source of GW170817 was found by Coulter et al. (2017) to be associated with the early-type galaxy NGC 4993 at a distance of about 40 Mpc, with the merger site located at a projected distance of about 2 kpc away from NGC 4993's galactic center. These observations would seem to favor a progenitor formed $\gtrsim$1 Gyr ago from an isolated binary in the field, receiving a natal kick velocity, V_k, of about 10^2 km s^{-1}

(Abbott et al. 2017d), as expected from merging neutron star models (Fryer & Kalogera 1998; Perna & Belczynski 2002; Kelley et al. 2010; Osłowski et al. 2011; Behroozi et al. 2014). Based on the inferred projected distance and the properties of the host (Abbott et al. 2017d), we expect the typical ambient density, $n_{\rm ext}$, in which the event occurred to be around $10^{-4}\,{\rm cm}^{-3}$ (Perna & Belczynski 2002), consistent with those inferred from afterglow modeling (e.g., Margutti et al. 2018).

If the binary progenitor of GW170817 hosted a pulsar, then a bow-shock cavity would have resulted from its interaction with the external medium, the characteristic size of which depends primarily on the premerger luminosity of the system. For an inspiraling binary with at least one pulsar, there are two widely commonly accepted mechanisms for energy dissipation. The first one is the traditional spin-down luminosity

$$L_{\rm p} \approx 1.5 \times 10^{35}\, B_9^{-2} \tau_{\rm p,9}^{-2}\ {\rm erg\ s^{-1}}, \quad (1)$$

where $\tau_{\rm p} = P/\dot{P}$ is the pulsar spin-down timescale ($\tau_{\rm p,9} = \tau_{\rm p}/10^9\,{\rm yr}$), B is the strength of the magnetic field ($B_9 = B/10^9\,{\rm G}$), and we have taken $R = 12\,{\rm km}$ and $M = 1.4 M_\odot$ as fiducial parameters.

The second one is the energy dissipation due to the torque on the binary by the magnetic field of the pulsar (Lai 2012),

$$L_{\rm B} \approx 7.4 \times 10^{36}\, \zeta_\phi B_9^2 a_{30}^{-13/2}\ {\rm erg\ s^{-1}}, \quad (2)$$

where ζ_ϕ is the azimuthal twist, which we take to be equal to the $\zeta_\phi \approx 1$ upper bound. This is because the flux tube will break up when $\zeta_\phi \gtrsim 1$ and, as a result, the linkage between the two binary components will be disconnected (Lai 2012). The orbital separation a ($a_{30} = a/30\,{\rm km}$), whose evolution is driven by gravitational-wave emission, is given by

$$a_{30} \approx \left(\frac{\tau_{\rm GW}}{1.2 \times 10^{-2}\ {\rm s}}\right)^{1/4}, \quad (3)$$

where $\tau_{\rm GW} = a/\dot{a}$ is the merging timescale.

The binary progenitor of GW170817 would have then formed a bow shock (Figure 1) with a characteristic size $R_{\rm s}$ given by (Wilkin 1996, 2000)

$$R_{\rm s} \approx 4.0 \times 10^{18}\, L_{35}^{1/2} n_{\rm ext,-4}^{-1/2} V_{\rm k,2}^{-1}\ {\rm cm}. \quad (4)$$

Here L is the isotropic luminosity ($L_{35} = L/10^{35}\,{\rm erg\ s^{-1}}$), $n_{\rm ext}$ is the number density of the medium ($n_{\rm ext,-4} = n_{\rm ext}/10^{-4}\,{\rm cm^{-3}}$), and $V_{\rm k,2} = V_{\rm k}/10^2\,{\rm km\ s^{-1}}$. Equation (4) becomes accurate in the limit of efficient cooling and is found to be in good agreement with sizes of cavities carved by anisotropic and nonaxisymmetric MHD pulsar winds (Vigelius et al. 2007; Barkov et al. 2019).

For small kick velocities ($V_{\rm k} \lesssim 10\,{\rm km\ s^{-1}}$), Equation (4) fails to provide an accurate description for the size of the cavity and a spherically symmetric solution becomes more accurate (Medvedev & Loeb 2013a, 2013b). However, given that the neutron star binary progenitor in GW170817 likely received a velocity in excess of $100\,{\rm km\ s^{-1}}$ (Abbott et al. 2017d), we expect Equation (4) to provide us with a reasonable estimate for the characteristic size of the evacuated region.

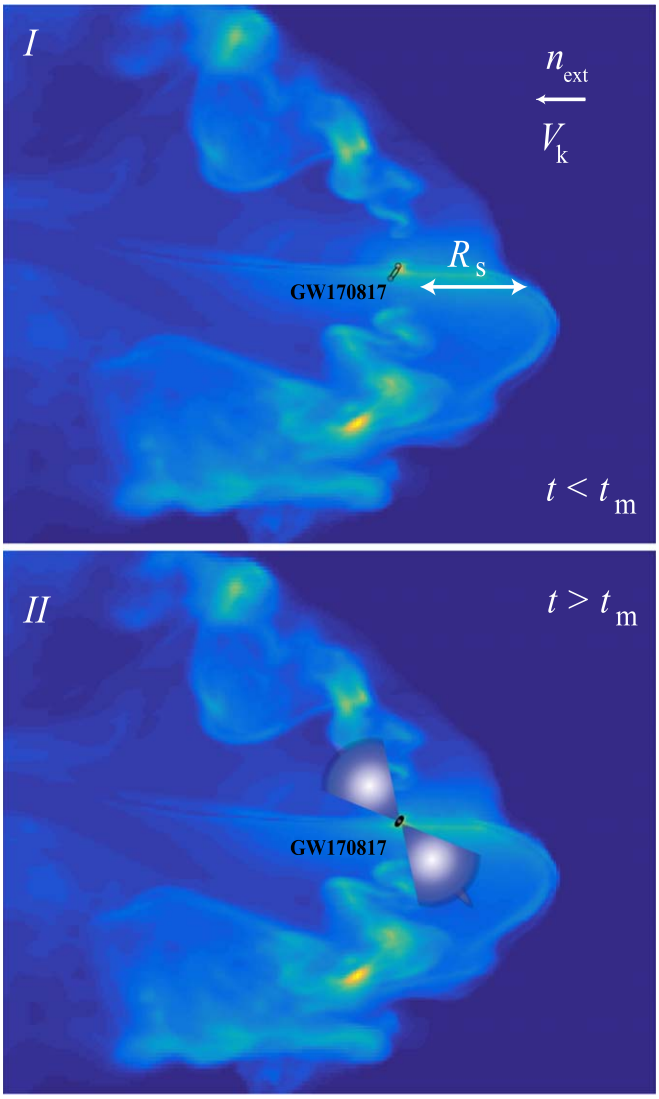

Figure 1. Diagram illustrating a typical cavity carved by an anisotropic and nonaxisymmetric MHD pulsar wind, adapted from Barkov et al. (2019). Panel I: $R_{\rm s}$ in the figure designates the characteristic scale (Equation (4)) at which the ram pressure of the wind is balanced by that of the external medium, with a number density $n_{\rm ext}$. The binary hosting the pulsar is assumed to be traveling through the external medium with a velocity $V_{\rm k}$ before the merger takes place (at $t = t_{\rm m}$). Panel II: swiftly after the merger, a relativistic jet is triggered, which is expected to have a complex angular structure. The deceleration of the jet at $R > R_{\rm s}$ is assumed to power the afterglow emission in GRB 170817.

3. Afterglows in Premerger Cavities and Implications for GRB 170817A

In the study of short γ-ray burst afterglows from neutron star mergers one commonly considers expansion into a uniform medium (e.g., Perna & Belczynski 2002). In the absence of a pulsar companion, the length scale of shock deceleration $R_{\rm dec}$ in the standard afterglow model (Rees & Meszaros 1992; Meszaros & Rees 1993) is given by

$$R_{\rm dec} \approx 1.6 \times 10^{18}\, E_{50}^{1/3} n_{\rm ext,-4}^{-1/3} \Gamma_5^{-2/3}\ {\rm cm}, \quad (5)$$

where $E_{50} = E/(10^{50}\,{\rm erg})$ is the isotropic-equivalent energy output of GRB 170817A and $\Gamma_5 = \Gamma/5$ is the bulk Lorentz factor. The values of E and Γ have been selected here to match those inferred (along our line of sight) from observations of GW170817 (Murguia-Berthier et al. 2017; Lazzati et al. 2018;

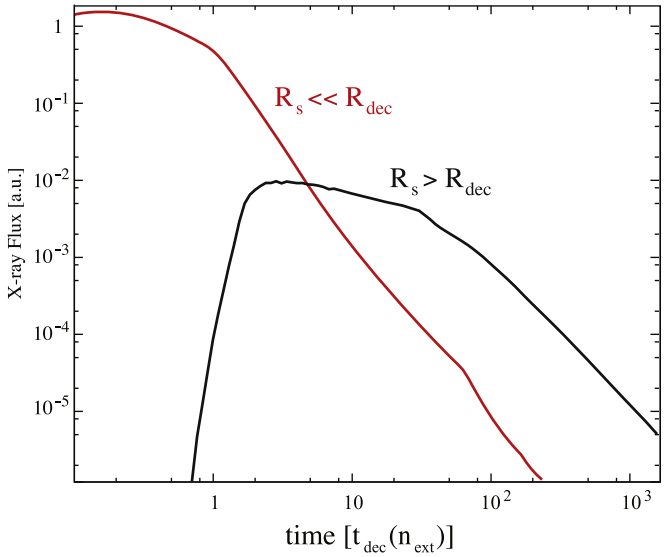

Figure 2. X-ray afterglow light curves (in arbitrary units, a.u.) from sGRBs triggered by neutron star mergers. For the red curve, the X-ray emission is computed for a standard sGRB blastwave expanding into a medium with constant density $n_{\rm ext}$. The blastwave is decelerated at $R_{\rm dec}(n_{\rm ext})$, which corresponds to $t_{\rm dec}$. The presence of a pulsar-wind cavity on the X-ray afterglow light curve can be seen by contrasting the red and black curves. In the pre-explosive cavity case, the blastwave expands freely within the cavity until it reaches the contact discontinuity at $R_{\rm s} = (5/2)\ R_{\rm dec}$. These spherical hydrodynamic models take on the density profile of the pulsar-wind cavity in the polar direction, as described in Holcomb et al. (2014), and provide a reasonable description of the observed afterglow properties for relativistic material expanding along our line of sight. Both calculations use the same microphysical parameters and assume $\Gamma = 10$. A detailed description of the numerical framework, light-curve calculations, and tests are presented in De Colle et al. (2012).

Margutti et al. 2018; Mooley et al. 2018; Matsumoto et al. 2019). This sets a characteristic deceleration time as measured by an observer along our line of sight (Rees & Meszaros 1992; Meszaros & Rees 1993; Zhang et al. 2006)

$$t_{\rm dec} = \left(\frac{1+z}{2}\right)\frac{R_{\rm dec}}{\Gamma^2 c} \approx 27.3\left(\frac{1+z}{2}\right)E_{50}^{1/3} n_{\rm ext,-4}^{-1/3}\Gamma_5^{-8/3}\ \text{days}. \quad (6)$$

The relativistic expansion is then gradually slowed down, and the blastwave evolves in a self-similar manner, as shown in the red curve of Figure 2. However, since the wind of the pulsar meets the interstellar medium at some point, the evolution of the blastwave can be modified, as shown in the black curve of Figure 2. In this case, the shock front expands unobstructed within the mass-evacuated pulsar-wind cavity until it reaches the contact discontinuity, which is placed here at $R_{\rm s} = (5/2)R_{\rm dec}(n_{\rm ext})$. The afterglow light curves presented in Figure 2 make use of the *Mezcal* special relativistic hydrodynamical calculations presented in Holcomb et al. (2014), in which we have assumed, for simplicity, that the blastwave is adiabatic and effectively spherical.

In general, if the premerger pulsar wind is weak enough that the blastwave would not be significantly slowed down by the time it expands beyond the pulsar-wind cavity $R_{\rm s} \ll R_{\rm dec}$, then we expect its evolution as we see it to take place in a uniform medium (red curve in Figure 2). Alternatively, we expect the presence of the pulsar-wind cavity to inevitably delay the onset of the afterglow when $R_{\rm s} \gtrsim R_{\rm dec}$ (black curve in Figure 2). It is thus useful to examine the range of conditions that fulfill this later requirement. Taking the ratio of Equations (4) and (5), we derive

$$\left(\frac{R_{\rm s}}{R_{\rm dec}}\right) \approx 2.5\, L_{35}^{1/2}\Gamma_5^{2/3}E_{50}^{-1/3}n_{\rm ext,-4}^{-1/6}V_{\rm k,2}^{-1}. \quad (7)$$

This ratio is modestly dependent on L and Γ, but weakly dependent on $n_{\rm ext}$ and E.

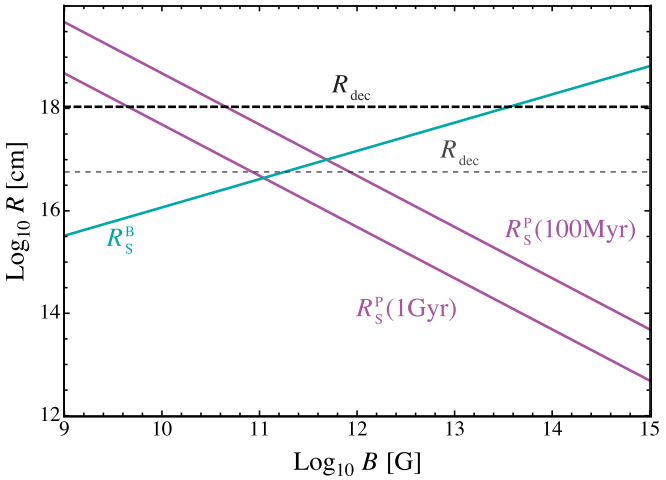

Figure 3. Properties of pre-explosive cavities in neutron star mergers with $V_{\rm k} = 100$ km s^{-1} and $n_{\rm ext} = 10^{-4}$ cm^{-3}. The relative contributions to $R_{\rm s}$ from $L_{\rm B}$ and $L_{\rm p}$ are plotted separately against the magnetic field strength of the pulsar. The purple lines indicate the contributions from $L_{\rm p}$ for $\tau_{\rm p} = 10^8$ yr and 10^9 yr, roughly corresponding to the range of expected merger delay times for GW170817 (Abbott et al. 2017d). The cyan line shows the expected contribution from $L_{\rm B}$ at the time of coalescence $\tau_{\rm GW} = 0$. For comparison, we plot $R_{\rm dec}(E_{50}, \Gamma_{10})$ as a black dashed line and $R_{\rm dec}(E_{52}, \Gamma_{300})$ as a gray dashed line, selected to roughly match the conditions inferred from the afterglow observations of GW170817 along our line of sight and for an on-axis observer, respectively (Lazzati et al. 2018; Margutti et al. 2018).

In Figure 3 we compare the relative contribution of $L_{\rm B}$ and $L_{\rm p}$ to $R_{\rm s}$ by separating it into $R_{\rm s}^{\rm B} = R_{\rm s}(L_{\rm B})$ and $R_{\rm s}^{\rm p} = R_{\rm s}(L_{\rm p})$. In order to calculate the size of the cavity produced by $L_{\rm B}$ we must make the transformation $\tau_{\rm GW} \rightarrow \tau_{\rm GW} + R_{\rm s}^{\rm B}/c$ in order to correctly compute $R_{\rm s}^{\rm B}$ (Holcomb et al. 2014). This is because $L_{\rm B}$ propagates to the bow-shock interface within a finite amount of time and there is a lag of $R_{\rm s}^{\rm B}/c$ before $R_{\rm s}^{\rm B}$ can react to changes in $L_{\rm B}$. For this reason, the size of the cavity at the time of merger (Equation (4)) should be computed using $L_{\rm B}$, which, after making the substitution that $a \sim (\tau_{\rm GW})^{1/4} \sim (R_{\rm s}^{\rm B}/c)^{1/4}$ in Equation (2), gives $R_{\rm s}^{\rm B} \propto B^{16/29}$ (Figure 3). We find that $L_{\rm p}$ dominates for most realistic values of B and $\tau_{\rm p}$, while $L_{\rm B}$ becomes only relevant when $B > 10^{12}$ G (likely to be unrealistic as it assumes no field decay). In addition, in Figure 3 we plot two values of $R_{\rm dec}$, corresponding to the deceleration radii inferred from afterglow observations of GW170817 (Lazzati et al. 2018; Margutti et al. 2018) along our line of sight (black dashed line) and along the jet's axis (gray dashed line), respectively. Since $R_{\rm s}$ can in some cases exceed $R_{\rm dec}$, we expect that afterglows emanating from neutron star mergers to noticeably trail the prompt emission, in particular when the observer is near the axis of the jet (e.g., Murguia-Berthier et al. 2014). We comment further on this in Section 4.

Observations summarized in Abbott et al. (2017b) show that the first detection of afterglow emission in GW170817 was

uncovered at $t = 9.2$ days at X-ray wavelengths. This can be used to set a constraint on the X-ray emitting radius, R_x, as measured by an observer along our line of sight:

$$R_{dec} \lesssim R_x \approx 5.5 \times 10^{17}\Gamma_5^2 \text{ cm}. \quad (8)$$

This in turn implies that the mass required to decelerate the ejecta was not pushed out beyond R_{dec} by the Poynting flux emanating from the pulsar companion and, as such, it suggests that $R_s \lesssim R_{dec} \lesssim R_x \approx 5.5 \times 10^{17}\Gamma_5^2$ cm. The fulfillment of the condition $R_s \lesssim R_x$ naturally translates into a limit on the premerger wind luminosity

$$L \lesssim 2 \times 10^{33}\Gamma_5^4 n_{ext,-4} V_{k,2}^2 \text{ erg s}^{-1}. \quad (9)$$

Here the bulk Lorentz factor (along our line of sight), Γ, is highly constrained by the condition that 2.3 days $\lesssim t_{dec} \lesssim$ 9.2 days (Margutti et al. 2018), which can be rewritten using Equation (6) as $1.1E_{50}^{1/8} n_{ext,-4}^{-1/8} \lesssim \Gamma_5 \lesssim 2.05E_{50}^{1/8} n_{ext,-4}^{-1/8}$. This is in agreement with arguments connected with the estimated opacity of the γ-ray emitting region (Matsumoto et al. 2019), for material moving along our line of sight.

The nondetection of the X-ray afterglow at 2.3 days can, in principle, be used to place tighter constraints on the characteristic size of the emitting region under the assumption that the afterglow data are consistent with a quasi-spherical, subenergetic explosion (Figure 2). However, given that the flow is likely to be collimated into jets (Lazzati et al. 2018; Margutti et al. 2018), the exact observed afterglow properties are expected to vary depending upon the angle, θ_{obs}, from the symmetry axis of the jet at which they are viewed. For example, if one assumes a homogeneous sharp-edged jet (Murguia-Berthier et al. 2017), an off-axis observer will see a rising afterglow light curve at early times (as the flow decelerates and the Lorentz factor decreases with time) peaking when the jet Lorentz factor reaches $\sim 1/\theta_{obs}$ and approaching that seen by an on-axis observer at later times. In this case, Equation (9) provides us with a conservative underestimate of the premerger wind luminosity.

The constraint on the premerger luminosity should be thus taken as an order of magnitude estimate at present and is currently consistent with the presence of an unrecycled (i.e., low-luminosity) pulsar. However, as we show below, it allows for meaningful constraints to be placed on the nature of a potential pulsar binary companion, in particular if the properties of the Galactic neutron star binaries are indicative of the general merging population. This is because a large number of Galactic systems would have been expected to carve discernible cavities. If merging binaries hosting low-luminosity pulsars are, on the other hand, common, then we expect no clear delay between the onset of the afterglow and the prompt emission.

In Figure 4 we translate the condition $R_s \lesssim R_x$ to constraints in the P–$\dot{P}$ diagram. The region of interest is separated into two distinct zones: low field pulsars with long spin-down timescales and high field pulsars. In the latter case, the necessary conversion $\tau_{GW} \rightarrow \tau_{GW} + R_s^B/c$ was made. For the low field pulsars, which depend on their spin to generate premerger luminosity, an additional constraint should be that $\tau_p \gtrsim \tau_{GW}$. For this reason, we have truncated the region of interest in Figure 4 to include low pulsar field systems with $\tau_p \gtrsim 10$ Myr as inferred from the typical merging times of double neutron star binaries (Figure 5). For high field pulsars, on the other hand, the constraints are independent of τ_p (Equation (2)). After translating the condition that $R_s \lesssim R_x$ into a constraint on

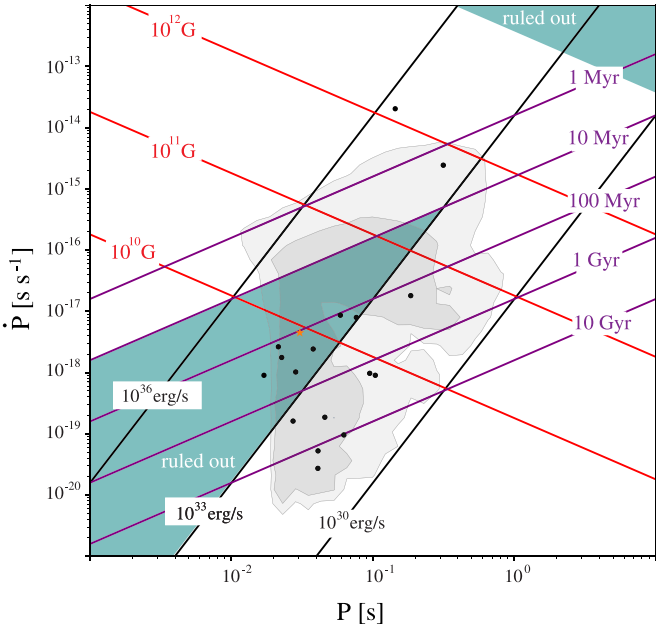

Figure 4. Constraints on the presence of a pulsar in GW170817 in the $P - \dot{P}$ diagram. Standard lines for τ_p (purple lines), pulsar magnetic field B (red lines), and spin-down luminosities L_p (black lines) are shown. The light blue shaded region indicates where the condition $R_s \gtrsim R_x$ is satisfied. To this end, we have adopted the fiducial values described in Equation (9) based on the afterglow solutions derived by Lazzati et al. (2018) and Margutti et al. (2018). For low field pulsars, we add the constraint that $\tau_p \gtrsim \tau_{GW} \gtrsim 10$ Myr, based on the typical merging times of double neutron star binaries. The gray contours represent the 2σ and 3σ contours for a neutron star binary to host a pulsar companion within the given region (Osłowski et al. 2011). Black symbols show the properties of the 17 observed pulsars in the field, while the yellow star symbol shows B2127+11C, a dynamically assembled system located in the globular cluster M15.

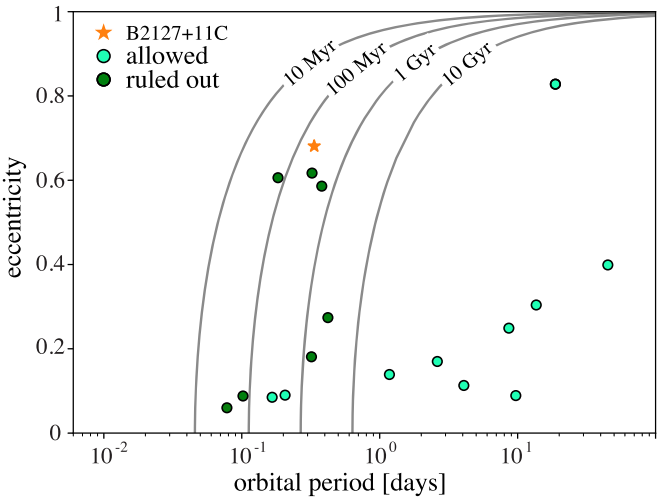

Figure 5. Orbital period and eccentricity distribution of the Milky Way DNSs, along with lines of constant merger time due to gravitational-wave radiation. Excluding those systems that are too widely separated merge within a Hubble time, only two Galactic DNSs fit the P–$\dot{P}$ constraints defined in Figure 4. We exclude one of these, J1906+0746, whose nature is unconfirmed, but likely hosts a recycled pulsar that is beamed away from Earth (van Leeuwen et al. 2015). The other system, J1913+1102 (Lazarus & Freire 2016; Ferdman & PALFA Collaboration 2018), provides a potential Milky Way analog to the progenitor of GW170817 (see Section 4).

the pulsar P–$\dot{P}$ diagram, Figure 4 shows that roughly half of all Milky Way double neutron star binaries fall outside the constraints. To get a sense for the likelihood that such systems are indeed representative, we have included in Figure 4 the contours from the double neutron star binary population synthesis modeling of Osłowski et al. (2011). With the caveat that the uncertainties of population synthesis are significant, a sizable fraction of binaries lie within the excluded region, and all of these systems are in the low field, long-lived pulsar branch.

4. Discussion

It is clear from the above discussion that the uniform environment expected to surround double neutron star binaries at the time of merger can be altered if the system hosts a pulsar. The spin-down luminosity of the pulsar companion is expected to be carried away in a magnetized wind that expands into the surrounding medium, decelerating as it sweeps up ejecta from the interstellar medium, eventually forming a bow-shock cavity. The onset of the afterglow can thus be noticeably delayed from the prompt emission if the size of the resultant cavity is larger than the shock deceleration length scale in the undisturbed interstellar medium. This condition is easily satisfied for high field pulsars $B \gtrsim 10^{13}$ G, irrespective of the spin-down age (Equation (2)). However, this is only valid under the assumption of no significant magnetic field decay. The processes regulating pulsar field decay are still highly debated, yet it is expected to occur on a timescale that is shorter then the lifetime of the system (Osłowski et al. 2011; Chashkina & Popov 2012; Igoshev et al. 2014; Klus et al. 2014). If, as expected, magnetic field decay occurs, then the pulsar lifetime $\tau_{\rm p}$ becomes a key parameter, as younger pulsars are expected to produce more extended cavities at a given magnetic field strength.

If the magnetic field strength does not change significantly with time, $L_{\rm p}$ can be written in terms of the pulsar's age (Equation (1)) by assuming that its initial period P_0 was much shorter than the current period. From dipole radiation we know that

$$\dot{P} = 9.8 \times 10^{-19} \left(\frac{B}{10^{10}\ \mathrm{G}}\right)^2 \left(\frac{P_0}{100\ \mathrm{ms}}\right)^{-1} \mathrm{s\ s^{-1}}. \quad (10)$$

Substituting this, along with $\tau_{\rm p} = P/\dot{P}$ for the spin-down luminosity, into Equation (4) we get

$$R_{\rm s} = 1.6 \times 10^{18} n_{\rm ext,\,-4}^{-1/2} V_{k,2}^{-1} B_{10} P_{0,-1}^{-2}\ \mathrm{cm}, \quad (11)$$

where $P_{0,\,-\,1} = P_0/100$ ms. Now, from Tauris et al. (2017) we have a relation between the (birth) spin period and the orbital period of the binary

$$P_0 = 36 \left(\frac{P_{\rm bin}}{\mathrm{days}}\right)^{0.4}\ \mathrm{ms}, \quad (12)$$

which, in turn, relates to the gravitational merger timescale

$$\tau_{\rm GW} = 0.0725 \left(\frac{P_{\rm bin}}{0.1\ \mathrm{days}}\right)^{8/3}\ \mathrm{Gyr}, \quad (13)$$

where we have assumed zero eccentricity, which provides a reasonable approximation for the merger time of most galactic double neutron star binaries.

Under this assumption, Equation (11) reduces to

$$R_{\rm s} = 3.5 \times 10^{18}\ n_{\rm ext,\,-4}^{-1/2} V_{\rm k,2}^{-1} B_9\ \tau_{\rm GW,\,Gyr}^{-0.3}\ \mathrm{cm}. \quad (14)$$

This implies that the eventual delay between the afterglow and the prompt emission $\approx R_s/(2c\Gamma^2)$ depends on the merging timescale, and, as such, offers a direct observational test on the assembly properties of the progenitor system. These constraints are likely to be more stringent for mergers in which the jet axis is near the observer's direction and the time delay between the prompt and afterglow emission is expected to be much shorter (Equation (6)).

Figure 5 shows the distribution of orbital periods and eccentricities for the 17 double neutron star binary population in the Milky Way field, as well as B2127+11C, a dynamically assembled system (Grindlay et al. 2006; Lee et al. 2010) located in the globular cluster M15. Lines of constant merger time due to gravitational-wave radiation are indicated in black; a sizable fraction of those have orbital periods too long for the systems to merge within a Hubble time due to gravitational-wave radiation; only two DNSs are allowed by the constraints on P and $\dot{P}$.[3] One of these is the unconfirmed double neutron star binary, J1906+0746, that hosts a young, unrecycled pulsar. Its companion could be a massive white dwarf, but is likely a recycled pulsar that is either too weak or beamed away from Earth (van Leeuwen et al. 2015). The other system that satisfies the P–$\dot{P}$ condition, the recently detected system J1913+1102 (Lazarus & Freire 2016; Ferdman & PALFA Collaboration 2018), provides a potential Milky Way analog of the progenitor of GW170817. Given the uncertainties in the afterglow modeling, we urge caution in the strict application of our results. For example, if the limit on the premerger wind luminosity given by Equation (9) is reduced by a factor of 6 (well within the derived uncertainties in our estimation of the size of the cavity), the two pulsars with merging ages between 1 and 10 Gyr in Figure 5 will be able to satisfy the revised constraints in the P–$\dot{P}$ plane. The precise measurement of the time delay between the prompt and afterglow emission can thus help provide key constraints on the premerger history of the binary system

4.1. PSR J1913+1102: A Milky Way Analog of the Double Neutron Star Progenitor of GW170817

Among the DNSs in the Milky Way, J1913+1102 is somewhat unique: whereas all other Galactic DNSs that will merge within a Hubble time have characteristic ages <0.5 Gyr, J1913+1102's characteristic age is 2.7 Gyr, a delay time of similar order to the last star formation episode of NGC 4993 (Hjorth et al. 2017; Im et al. 2017; Palmese et al. 2017). Furthermore, its P and $\dot{P}$ translate to $L \approx 5 \times 10^{32}$ erg s^{-1} and $B \approx 2 \times 10^9$ G, characteristics that fit within the constraints we place here based on the ≈9 day delay between the arrival of the prompt emission and the onset of the afterglow. These constraints were derived assuming a peculiar velocity of 100 km s^{-1}. A dispersion-measure-derived distance combined with a proper motion measurement of J1913+1102 indicates it is moving with a tangential velocity of ≈400 km s^{-1}; however, without knowledge of the system's radial velocity it is difficult

[3] This is a relatively robust result. If, for example, the derived limit on the premerger luminosity was an order of magnitude less stringent (based on the uncertainties associated with $n_{\rm ext}$ and $V_{\rm k}$), only two additional systems will be allowed by the P and $\dot{P}$ constraints.

to determine the velocity of J1913+1102 relative to the local standard of rest.

Despite this caveat, J1913+1102 produces one of the best Milky Way analogs currently available with which to compare to the progenitor of GW170817. Besides satisfying the total mass requirements (as most other Galactic neutron star binaries; Abbott et al. 2017a), J1913+1102 is a large mass ratio ($q \approx 1.35$) system, suggesting a larger amount of tidal ejecta upon merger as estimated for GW170817 (Kasen et al. 2017; Kilpatrick et al. 2017). This analysis highlights the potential of the observational tool presented in this Letter. Space- and ground-based observations over the coming years should allow us to uncover the detailed nature of these most remarkable binaries.

We are especially grateful to C. Holcomb and F. De Colle for extended collaboration and V. Kaspi and S. Ransom for discussions. We also thank the referee for many useful suggestions improving the exposition of this Letter. We are indebted to the David and Lucile Packard Foundation, the Heising-Simons Foundation, the Danish National Research Foundation (DNRF132), and NSF (AST-1911206) for support.

ORCID iDs

Enrico Ramirez-Ruiz https://orcid.org/0000-0003-2558-3102
Jeff J. Andrews https://orcid.org/0000-0001-5261-3923
Sophie L. Schrøder https://orcid.org/0000-0003-1735-8263

References

Abbott, B. P., Abbott, R., Abbott, T. D., et al. 2017a, PhRvL, 119, 161101
Abbott, B. P., Abbott, R., Abbott, T. D., et al. 2017b, ApJL, 848, L12
Abbott, B. P., Abbott, R., Abbott, T. D., et al. 2017c, ApJL, 848, L13
Abbott, B. P., Abbott, R., Abbott, T. D., et al. 2017d, ApJL, 850, L40
Barkov, M. V., Lyutikov, M., & Khangulyan, D. 2019, MNRAS, 484, 4760
Behroozi, P. S., Ramirez-Ruiz, E., & Fryer, C. L. 2014, ApJ, 792, 123
Burgay, M., D'Amico, N., Possenti, A., et al. 2003, Natur, 426, 531
Chashkina, A., & Popov, S. B. 2012, NewA, 17, 594
Coulter, D. A., Foley, R. J., Kilpatrick, C. D., et al. 2017, Sci, 358, 1556
De Colle, F., Granot, J., López-Cámara, D., & Ramirez-Ruiz, E. 2012, ApJ, 746, 122
Ferdman, R. D., et al. PALFA Collaboration 2018, in IAU Symp. 337, Pulsar Astrophysics the Next Fifty Years 337, ed. P. Weltevrede (Cambridge: Cambridge Univ. Press), 146
Fryer, C., & Kalogera, V. 1998, ApJ, 499, 520
Grindlay, J., Portegies Zwart, S., & McMillan, S. 2006, NatPh, 2, 116
Hjorth, J., Levan, A. J., Tanvir, N. R., et al. 2017, ApJL, 848, L31
Holcomb, C., Ramirez-Ruiz, E., De Colle, F., & Montes, G. 2014, ApJL, 790, L3
Hulse, R. A., & Taylor, J. H. 1975, ApJL, 195, L51
Igoshev, A. P., Popov, S. B., & Turolla, R. 2014, AN, 335, 262
Im, M., Yoon, Y., Lee, S.-K. J., et al. 2017, ApJL, 849, L16
Kalogera, V., Narayan, R., Spergel, D. N., et al. 2001, ApJ, 556, 340
Kasen, D., Metzger, B., Barnes, J., Quataert, E., & Ramirez-Ruiz, E. 2017, Natur, 551, 80
Kelley, L. Z., Ramirez-Ruiz, E., Zemp, M., Diemand, J., & Mandel, I. 2010, ApJL, 725, L91
Kilpatrick, C. D., Foley, R. J., Kasen, D., et al. 2017, Sci, 358, 1583
Kim, C., Perera, B. B. P., & McLaughlin, M. A. 2015, MNRAS, 448, 928
Klebesadel, R. W., Strong, I. B., & Olson, R. A. 1973, ApJL, 182, L85
Klus, H., Ho, W. C. G., Coe, M. J., Corbet, R. H. D., & Townsend, L. J. 2014, MNRAS, 437, 3863
Lai, D. 2012, ApJL, 757, L3
Lattimer, J. M., & Schramm, D. N. 1976, ApJ, 210, 549
Lazarus, P., Freire, P. C. C., Allen, B., et al. 2016, ApJ, 831, 150
Lazzati, D., Perna, R., Morsony, B. J., et al. 2018, PhRvL, 120, 241103
Lee, W. H., Ramirez-Ruiz, E., & van de Ven, G. 2010, ApJ, 720, 953
Margutti, R., Alexander, K. D., Xie, X., et al. 2018, ApJL, 856, L18
Matsumoto, T., Nakar, E., & Piran, T. 2019, MNRAS, 483, 1247
Medvedev, M. V., & Loeb, A. 2013a, ApJ, 768, 113
Medvedev, M. V., & Loeb, A. 2013b, MNRAS, 431, 2737
Meszaros, P., & Rees, M. J. 1993, ApJ, 405, 278
Mooley, K. P., Deller, A. T., Gottlieb, O., et al. 2018, Natur, 561, 355
Murguia-Berthier, A., Montes, G., Ramirez-Ruiz, E., De Colle, F., & Lee, W. H. 2014, ApJL, 788, L8
Murguia-Berthier, A., Ramirez-Ruiz, E., Kilpatrick, C. D., et al. 2017, ApJL, 848, L34
Osłowski, S., Bulik, T., Gondek-Rosińska, D., & Belczyński, K. 2011, MNRAS, 413, 461
Palmese, A., Hartley, W., Tarsitano, F., et al. 2017, ApJL, 849, L34
Perna, R., & Belczynski, K. 2002, ApJ, 570, 252
Rees, M. J., & Meszaros, P. 1992, MNRAS, 258, 41P
Scholz, P., Kaspi, V. M., Lyne, A. G., et al. 2015, ApJ, 800, 123
Stovall, K., Freire, P. C. C., Chatterjee, S., et al. 2018, ApJL, 854, L22
Tauris, T. M., Kramer, M., Freire, P. C. C., et al. 2017, ApJ, 846, 170
van Leeuwen, J., Kasian, L., Stairs, I. H., et al. 2015, ApJ, 798, 118
Vigelius, M., Melatos, A., Chatterjee, S., Gaensler, B. M., & Ghavamian, P. 2007, MNRAS, 374, 793
Wilkin, F. P. 1996, ApJL, 459, L31
Wilkin, F. P. 2000, ApJ, 532, 400
Wong, T.-W., Willems, B., & Kalogera, V. 2010, ApJ, 721, 1689
Zhang, B., Fan, Y. Z., Dyks, J., et al. 2006, ApJ, 642, 354